

A Unified Classification Framework with Quantum Metric Learning

Nhat A. Nghiem,¹ Samuel Yen-Chi Chen,² and Tzu-Chieh Wei^{3,1}

¹*Department of Physics and Astronomy, State University of New York at Stony Brook, Stony Brook, NY 11794-3800, USA*

²*Computational Science Initiative, Brookhaven National Laboratory, Upton, NY 11973, USA*

³*C. N. Yang Institute for Theoretical Physics, State University of New York at Stony Brook, Stony Brook, NY 11794-3840, USA*

Recently, Lloyd et al. [arXiv:2001.03622] introduced *quantum metric learning* as a powerful framework for quantum supervised learning. Such strategy focuses on the training of the quantum embedding, with a goal of ‘well-separation’ of the embedded data in the Hilbert space \mathcal{H} . Motivated by such an idea, we present a metric-based framework for supervised learning with trainable quantum circuits. We introduce both explicit and implicit approaches, based on the *metric* defined on the Hilbert space \mathcal{H} , to classify data. In particular, with the implicit approach, the number of separated classes (or their labels) in supervised learning problems can be arbitrarily high (with respect to the number of given qubits, or more precisely, the number of measurement), which is an improvement over current quantum supervised learning models, and this approach requires relatively small number of training points. With the explicit approach, we establish an equivalence between our metric-based framework and other quantum supervised learning models. Such equivalence provides a unification of supervised learning frameworks on quantum computer. We also demonstrate our framework by performing both noise-free and noisy numerical simulations and by running the classification on real IBM Q devices.

I. INTRODUCTION

Quantum computation has been intensively studied over the past few decades and it is expected to outperform its classical counterpart in certain computational tasks [1, 2]. In such a novel approach of computation, information is stored in the quantum states of an appropriately chosen and designed physical system, which reside in a complex Hilbert space \mathcal{H} , and quantum bits (qubits) are conveniently used as the underlying building blocks and the processing units. The power of a quantum computer lies in the ability to store and process information coherently in the tensor-product Hilbert space [1], with entanglement being a characteristic byproduct or even a potential resource of quantum information processing [3, 4]. Quantum computation have been shown to provide dramatic speedup in solving some important computational problems, such as factorization of a large number via Shor’s algorithm [5] and the unstructured search via Grover’s algorithm [6], as two prominent examples of many that have been discovered.

At the same time, machine learning (ML) has become a powerful tool in modern computation. For example, ML has been successful in computer vision [7–9], natural language processing [10], drug discovery [11] and even in playing the game of Go [12]. It is thus a natural application of quantum computers which may also provide substantial speedup [13–16]. Quantum computing can potentially benefit various tasks in ML, from dividing data into clusters, learning patterns for facial/speech recognition, or performing sequential decision making, where a vast amount of data needs to be stored and processed. Several previous works have demonstrated quantum advantages in the field of unsupervised learning [17–21]. For example, in Ref. [20], the authors provided quantum algorithms for clustering problems (an instance of unsupervised learning), which yielded exponential speedup in

principle. In Ref. [21], the authors introduced a quantum version of k-means clustering, namely, q-means and presented an efficient quantum procedure.

The use of quantum computation in supervised learning has also received increasing attention [22, 23]. For example, the authors of Ref. [24] presented a quantum version of support vector machines (SVM) and showed possible exponential speedup. For near-term applications, variational strategies have been proposed to classify real-world data [22, 25–28]. In fact, classification is one of the standard problems in supervised learning [29, 30], and variational methods using short-depth quantum circuits with trainable parameters, such as rotational angles of single-qubit gates, give rise to a quantum-classical hybrid optimization procedure. Such a framework has been shown to be capable of performing complex classification tasks [25, 26, 28, 31], and many more to appear. It has also been shown that such variational methods are capable of learning complex representations while still being robust to noise in near-term quantum devices (NISQ) [28, 32]. The classification procedure with quantum circuits has two key steps: (1) Perform a quantum feature mapping; (2) Perform appropriate measurement. The outcome of the measurement is usually interpreted as the output of the learning model. The quantum feature mapping has a surprisingly deep connection to the classical kernel method, and has been formally established in Ref. [33]. Various embedding methods, such as basis, amplitude, variational and product encoding [22], have been employed in many contexts and are crucial for the design of quantum architectures [34]. For example, in Ref. [35], the authors use the basis encoding scheme to tackle the deep *Q*-learning problem, while in Ref. [36], the authors apply variational encoding to construct a hybrid quantum-classical architecture which is capable of learning the temporal/sequential data.

A clear picture thus emerges in the quantum super-

vised learning: a feature map first embeds classical data x into some quantum state $|x\rangle$, i.e., a data point in Hilbert space \mathcal{H} . This space is also called the quantum feature space, an analogous to the feature space in classical machine learning setting. Then a decision boundary is learnt by training the variational circuit to adapt the measurement basis. In Ref. [37], the authors emphasize the training of the embedding part and propose a strategy called quantum metric learning, with inspiration from classical metric learning [38]. They employ a quantum classifier which has the output of the form $f(x) = \langle x | M | x \rangle$ (M is Hermitian operator). They consider two types of measurements: (a) the fidelity measurement, where $M = \rho - \sigma$, and (b) the Helstrom measurement, where $M = \Pi_+ - \Pi_-$. In their context, ρ and σ are the ensemble of embedded data from different classes, and Π 's are the sum of projectors to positive/negative subspace of $\rho - \sigma$, respectively (see Ref. [37] and Appendix A for details). The optimization procedure would then separate two data classes with either trace distance (also called l_1 distance) or Hilbert-Schmidt distance (l_2). The trained quantum circuit maps classical data points to two ‘sides’ of the Hilbert space \mathcal{H} . Such a method is nevertheless limited to the binary classification. Even though in practice, a binary classifier can be turned into multi-classifier by using one-versus-all strategy, however, clearly more resources are required to train and store learning parameters, and thus more quantum operations are required to classify unseen data. In the near-term noisy era of quantum processors, access to quantum resources should be minimized. In fact, in a more restricted view, a model that can deal with multi-classification is systematically different from a model that can only perform binary classification. Hence, motivation for our work comes from the concern of whether or not such quantum metric learning strategy can be expanded directly to the multi-label case, as well as any possibly further consequences of this embedding-focused strategy.

Inspired by the work of [37] and, in particular, the concept of ‘well-separation’, this work presents a unified metric-based framework for classification with quantum circuits. We shall divide our framework into explicit and implicit approaches. They are described below in detail and are backed up further by numerical simulations and tested on real quantum devices. The main intuition behind our framework is the observation of a possible correspondence between the input space of the data \mathcal{X} and the Hilbert space \mathcal{H} of the embedded data. Data from the same class is considered to be similar in the input space and such similarity, at the core of our framework, is reflected in the corresponding Hilbert space. The motivation behind the idea of similarity reflection is inspired by the concept of clusters in machine learning. The goal is to train the embedding circuit so as to produce well-separated clusters of different labels. In our *implicit* approach, the ‘centers’ of these clusters are random. In contrast, in our *explicit* approach, the ‘centers’ are constrained to lie in or nearby some subspaces of the Hilbert

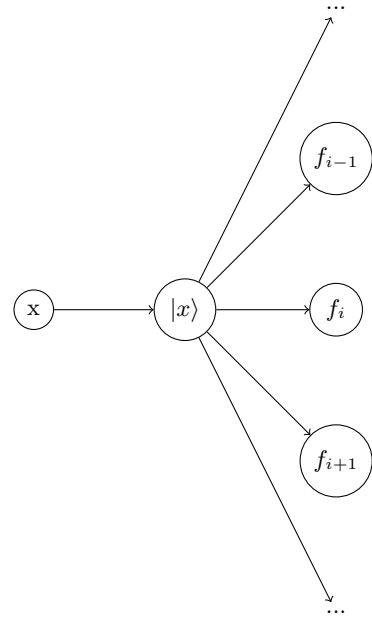


FIG. 1: **Metric-Forwarding Diagram** The input data x is mapped to quantum state $|x\rangle = \Phi(x, \theta)|0\rangle$, which is then used to calculate the *metric vector* $\vec{f}(x, \theta) \in \mathbb{R}^M$. The form of $\{f_i\}$ is specified by some metric \mathcal{M} . Classification is done based on values of $\{f_i\}$.

space. Similarity or distance measures have been defined and used widely in classical machine learning context. In our work, *metric* simply refer to such similarity measures. We will show that by employing chosen metric, one can draw a connection between \mathcal{X} and \mathcal{H} and this results in a direct means for classification.

The structure of the paper is as follows. In section II, we present a diagrammatic picture, which is the main conceptual tool, of our framework. In section III and IV, we discuss implicit and explicit approaches, respectively, and present results from numerical experiments and runs from real devices. We conclude in Sec. VI. In Appendix A, we show that in case of binary classification, the implicit approach would then focus on maximizing Hilbert-Schmidt distance between two data classes, as highlighted in [37]. We make some further comments on trace distance in Appendix B. In Appendix C, we discuss a remarkable consequence of focusing on embeddings part instead of measuring part in quantum classification.

II. GENERAL FRAMEWORK

We first introduce the general framework, which can be illustrated by the so-called metric-forwarding diagram, shown in Fig. 1. In the supervised learning problem with M separated labels, we are given a training set with corresponding labels $X \times Y = \{x, i\}$ where

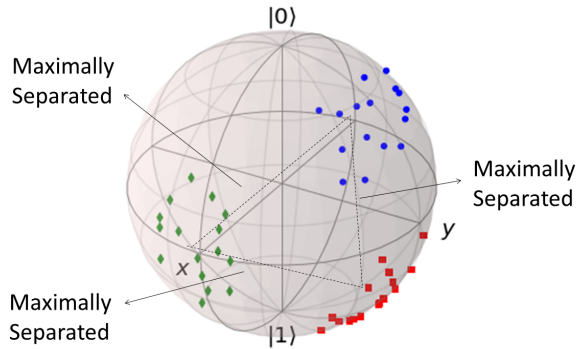


FIG. 2: **Illustration of implicit approach.** After training procedure, the ‘distance’ between any clusters (represented by dot lines) becomes maximal. The ‘center’ of each clusters are not fixed, as the training process will move them to produce well-separated clusters. *Note:* the data points in this picture are not related to the Iris dataset in our subsequent experiment, nor the data points in Fig. 11

$i \in \{0, 1, \dots, M-1\}$ is the label of the data point x . We need to predict a label for some other unseen data x . In quantum context, we simply use quantum representation $|x\rangle$ instead of x . The number of components $\{f_i\}$, or equivalently the dimension of $\vec{f}(x, \theta)$ is equal to M . The value f_i (for convenience, assumed to be in the range $0 \leq f_i \leq 1$) has a very important meaning: it quantifies the possibility that some input x having any of labels $\{i\}$. In this sense, the metric-forwarding diagram is somehow similar to the classical neural network, where the information is fed forward from the input layer to the output layer. There have been numerous works that explore the relation between quantum computation and neural network [25, 26, 39, 39–42]. The key relation comes from the building block of the quantum circuit model: quantum gates—which carry out unitary transformation on the input quantum state, which is a vector in some Hilbert space \mathcal{H} . In graphical representation (nicely illustrated in Ref. [26]), the action of a quantum gate on the input state $|\psi\rangle$ produces an output state $|\rho\rangle$ and can be represented as a fully connected two-layer network. Hence, a full quantum circuit can generally be represented by such a fully connected network with certain number of layers. Measuring quantum states then corresponds to a non-linear activation function.

Thus, in order to make prediction, we ‘forward’ x to such metrics vector $\vec{f}(x, \theta)$ and to it assign a label according to the highest value of f_i . The accuracy of correct assignment depends on the parameters θ . Now we give a strategy to train the circuit in order to obtain the parameters $\vec{\theta}$ that produce accurate classification. Ideally, we would want to maximize the similarity (quantified by some metric) among the data with the same label, and minimize the similarity between the data with different labels. For each label i , assume there are N_i training

points with such a label, and that there are totally N data points, where $N = \sum_i N_i$. Let \vec{y}_i be the real, so-called label vector of class i (which has dimension M) with components $\{y_i^j\}_{j=1}^M = \delta_{ij}$, where δ_{ij} is the Kronecker delta function. Let f_i^j be the metric-vector of j -th data. We minimize the following cost function:

$$C = \frac{1}{M} \sum_{i=1}^M \frac{1}{N_i} \sum_{j=1}^{N_i} |\vec{f}(x_i^j, \theta) - \vec{y}_i| \quad (1)$$

where x_i^j is the j -th data point in class i . The term $|\vec{f}(x_i^j, \theta) - \vec{y}_i|$ is \mathcal{L}_1 distance on real vector space between \vec{f}_i and \vec{y}_i . We note that any reasonable form of the loss function should work. However, the reason we use this particular L_1 loss is for the simplification of the cost in Eq. (6) below, for which certain advantages can be gained, as we will explain later.

Overlaps-Metric: Given two *pure* quantum states represented by density matrix $\rho \equiv |\rho\rangle\langle\rho|$ and $\phi \equiv |\phi\rangle\langle\phi|$. A similarity measure, thereby, a metric, on these two states can be given by $\text{Tr}(\rho\phi) = |\langle\rho|\phi\rangle|^2$. We refer to such metric as overlaps-metric. In the general case of mixed states, the SWAP test (ST) quantum procedure [1] can evaluate $\text{Tr}(\rho\phi)$ up to an additive error ϵ . In the special case of pure states, the *inversion test* (IT) [37] can be used to evaluate the overlaps between two quantum states $|\langle\phi|\cdot|\rho\rangle|^2$, provided that the circuit U to create either $|\phi\rangle$ or $|\rho\rangle$ can be efficiently inverted. Both schemes require only shallow circuits. In subsequent experiments, we thus use the overlap-metrics, as it is suitable for both simulations and near-term applications. We would also implement both schemes for classification on real devices.

III. IMPLICIT APPROACH

In this section, we first give construction of the implicit approach. In this approach, the data from the same class, after going through the quantum circuit $\Phi(x, \theta)$, produce clusters (closed data points) in the Hilbert space \mathcal{H} , and those clusters corresponding to different classes should become maximally separated after minimizing the cost function (see Fig. 2). Due to such feature, this approach can work well with a small number of training points. We will present numerical experiments for training and then examine the classifier with both noise-free, noisy simulators, and on real quantum ‘backends’. In latter experiments, we use fix optimal circuit parameters obtained in the ideally trained model and use the resultant network to test the classification of unseen data with noisy simulators and on real ‘backends’.

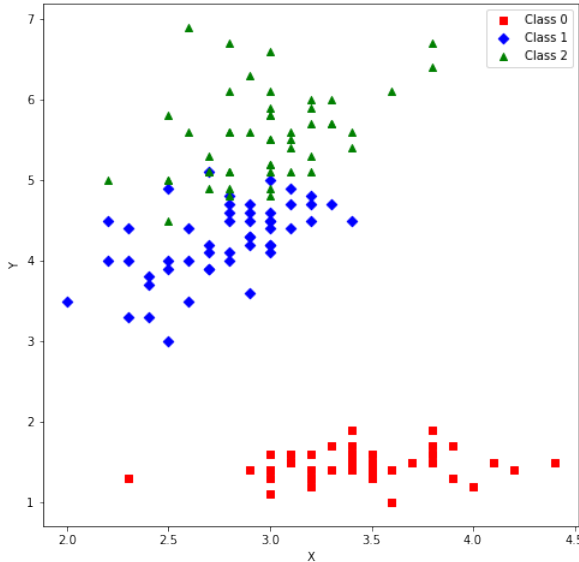


FIG. 3: The Iris Dataset. There are three classes distributed in a two-dimensional region. This will be used in our implicit approach for classification.

A. Description

To describe our supervised learning problem, we assume that for each label i , there are N_i training points that will be transformed to quantum states $\{|x_i^j\rangle\}_{j=1}^{N_i}$. Using overlaps-metric, the ‘distance’ between some input data $|x\rangle$ and $|x_i^j\rangle$ is $\text{Tr}(|x\rangle\langle x| |x_i^j\rangle\langle x_i^j|)$. As mentioned, the value of f_i infers the likelihood of $|x\rangle$ having label i . Such likelihood can be quantified by averaging ‘distances’ from $|x\rangle$ to all data points in i . Hence, f_i becomes:

$$f_i = \frac{1}{N_i} \sum_j \text{Tr}(|x\rangle\langle x| |x_i^j\rangle\langle x_i^j|) \quad (2)$$

which could also be written as:

$$f_i = \text{Tr}(|x\rangle\langle x| \sigma_i) \quad (3)$$

where σ_i is the ensemble corresponding to label i :

$$\sigma_i = \frac{1}{N_i} \sum_{j=1}^{N_i} |x_i^j\rangle\langle x_i^j|. \quad (4)$$

This ensemble could be interpreted as the collection of the corresponding training points from class i on \mathcal{H} , which can be obtained by sampling from the training set $\{x_i^j\}_{j=1}^{N_i}$. The metric vector $\vec{f}(x, \theta)$ now becomes:

$$\begin{bmatrix} \text{Tr}(|x\rangle\langle x| \sigma_0) \\ \text{Tr}(|x\rangle\langle x| \sigma_1) \\ \vdots \\ \text{Tr}(|x\rangle\langle x| \sigma_{M-1}) \end{bmatrix}. \quad (5)$$

We will focus on minimizing/maximizing those quantities $\{f_i\}$, and rely on such values to assign a label to x .

After applying Eq. (1), the cost function becomes

$$C = 1 - \frac{1}{M} \sum_{i=1}^N \text{Tr} \sigma_i^2 + \frac{2}{M} \sum_{i < j} \text{Tr} \sigma_i \sigma_j, \quad (6)$$

We note that the cross terms,

$$\text{Tr}(\sigma_i \sigma_j) = \frac{1}{N_i N_j} \sum_{k=1}^{N_i} \sum_{p=1}^{N_j} |\langle x_i^k | \cdot | x_j^p \rangle|^2, \quad (7)$$

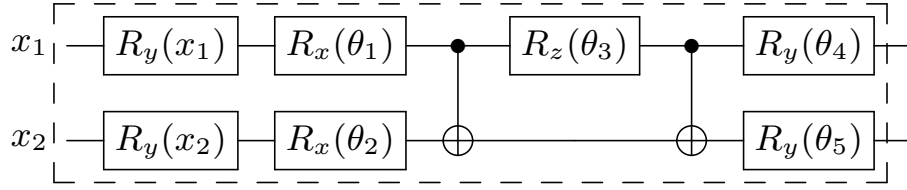
is a sum of the modulus square of overlaps. Hence, in the training produce, we can use either the SWAP test or inversion test to evaluate the cost.

Speedup with QRAM: If the quantum random access memory (QRAM) [44] is available, the cost for training and testing procedure will be reduced by a factor $\sim \sum_{i < j} N_i N_j$ and $\sum_i N_i$, respectively, where N_i is the number of the data points in each training set i . The calculation of cost function and classification of data can be done in time $\mathcal{O}(1)$. One could load the data corresponding to class i to a quantum state $|\psi_i\rangle = \frac{1}{\sqrt{N_i}} \sum_{j=1}^{N_i} |x_i^j\rangle |j\rangle$, where the index j represents the address of the memory where x_i^j is residing. The application of $R_y(x)$ then can be done by performing a conditional rotation $c - R_y(x)$ dependent on the third register and then tracing out the first two registers. In this way, at the expense of more complicated circuit to perform conditional rotation, and we do not need to perform sampling from the training set to obtain σ_i , which requires already-available states $\{|x_i\rangle\}$, nor do we need to calculate the overlap between all pairs in the sum; see Eq. (7). A possibly useful work is whether or not one can design an efficient quantum subroutine of low-depth circuits to evaluate the cost in Eq. (6) directly, so as to reduce the iterative evaluation steps. A relevant work to this question has been carried out in Ref. [45].

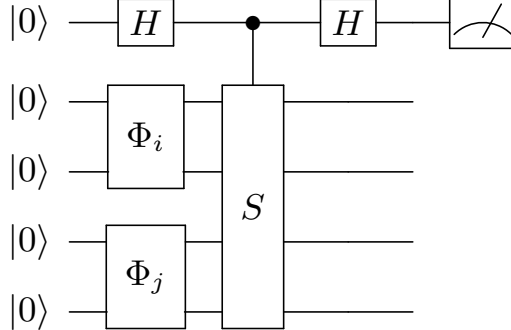
The particular form of the cost function in Eq. (6) has further consequence: it makes our classification model match perfectly with the quantum learning context. In this problem, the data is already available in quantum representation (in the form of either pure states or mixed states). One can just let such instances go through the circuit to obtain the corresponding fidelity and hence the cost. The availability of quantum data can reduce the circuit’s depth (for classical feature embeddings) and potentially overcome the need for QRAM. We finally note that our model can gain advantages dealing with tensor-based classical information, such as a 2D images, which generally can be encoded in some density matrix ρ in principle.

B. Numerical Simulations—the procedure

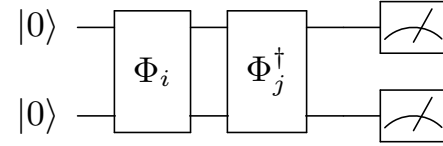
Datasets: For illustration purpose, we target the Iris dataset [46, 47] with $M = 3$ labels (see Fig. 3). There



(a) **Quantum Embedding Circuit Φ .** In our work, the rotational layer is repeated 4 times. Hence, the total number of trainable parameters are 20. In the end, the feature layer is repeated. The repetition of both feature layer and parameter layer has been quoted in [43] as data re-uploading strategy, and shown to yield better classification ability.



(b) **SWAP Test circuit.** $\Phi_{i,j}$ is the shorthand notation for embeddings two data instances i and j , respectively. Then the overlaps between any pair of data can be evaluated in this subroutine. With QRAM, if we neglect the loading cost, the average overlaps between two data classes can be done in time $\sim \mathcal{O}(\frac{1}{\epsilon^2})$ where ϵ is the additive error in the overlaps estimation, which is independent of size of given data classes.



(c) **Inversion Test circuit.** In our work, the embeddings circuit $\Phi(x, \theta)$ is invertible. The overlaps between two data points can be evaluated with fewer qubits.

FIG. 4: **Description of quantum embeddings circuit and two alternative methods to evaluate overlaps between two arbitrary pair of data points**

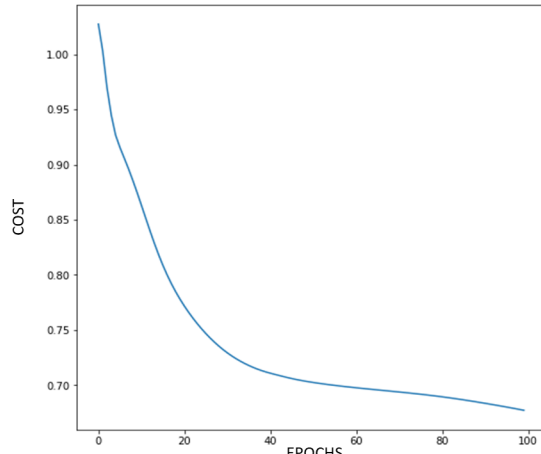


FIG. 5: **Cost as Function of Epochs.** In this training, we use 100 epochs. There are 10 training points for each class, hence, a total of 30 training points.

are 50 data points in each class, hence totally $N = 150$ data points. 10 data points are taken from each class to serve as the training data, and the remaining 40 are used for testing. Aside from classification, our aim is also to

demonstrate the formation of clusters in featured Hilbert space \mathcal{H} .

Quantum Embeddings: We use the same, so-called QAOA-like ansatz as in [37] (see Fig. 4a) for the embedding purpose. The circuit $\Phi(x, \theta)$ is composed of a feature layer $U(x)$ followed by the parameter layer $W(\theta)$, and hence we have $\Phi(x, \theta) = W(\theta)U(x)$. $\Phi(x, \theta)$ is then repeated 4 times, with additional feature layer $U(x)$ at the end. Generally, results produced by this QAOA-like ansatz is inaccessible to classical computers, which was also elaborated in [37].

Training Stage: Since there are $N = 3$ labels in our problem, the cost function is:

$$C = 1 - \frac{1}{3} \sum_{i=1}^3 \text{Tr}(\sigma_i)^2 + \frac{2}{3} \sum_{i < j} \text{Tr}(\sigma_i \sigma_j). \quad (8)$$

The procedure of the training is as follows.

- Data from the training set is mapped to quantum states.
- Define and use SWAP test subroutine to evaluate $\text{Tr}(\sigma_i^2)$ and $\text{Tr}(\sigma_i \sigma_j)$. Later, we also use inversion test.

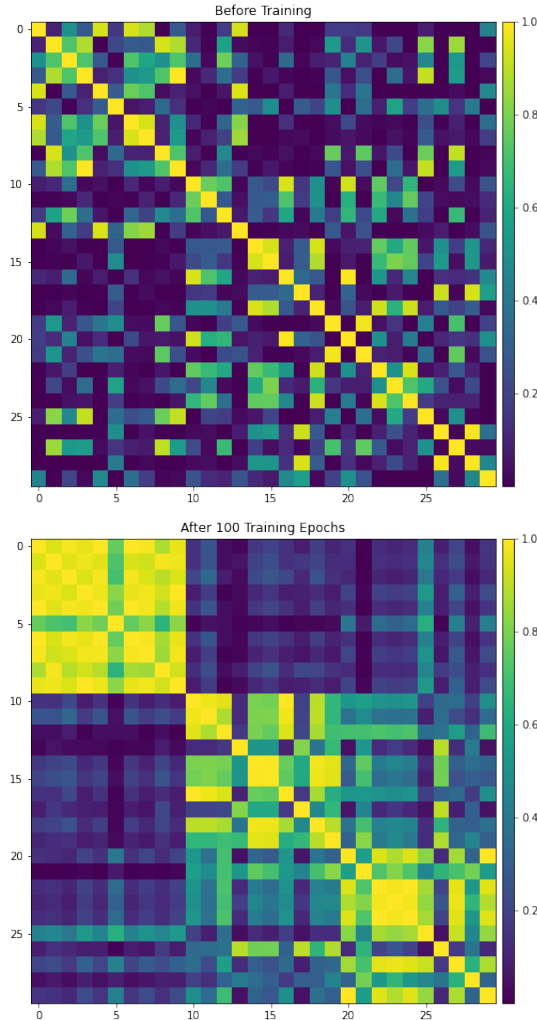


FIG. 6: **Visualization of overlaps between training points (10 training points in each class).**

(a) Top panel: Initial distribution of data in \mathcal{H} , in which the parameters in the variational quantum circuit were randomized. (b) Bottom panel: After 100 training epochs, the data from the same classes form a cluster on \mathcal{H} , as overlaps between their quantum states are high (brighter color). The visualization clearly shows that class 0 (red points) are much separated from other two classes. Meanwhile, class 1 (blue points) and 2 (green points) are less well-separated from each other.

Such observation is in agreement with the testing results, as all testing points from class 0 are predicted with absolute accuracy, and false predictions mainly come from class 1 and 2.

- Minimize the cost C in Eq. (8) over circuit parameters.

The simulation uses the PennyLane software package [48] and the optimization of C over circuit parameters is done with the RMSprop [49] optimizer with a learning rate of 0.01.

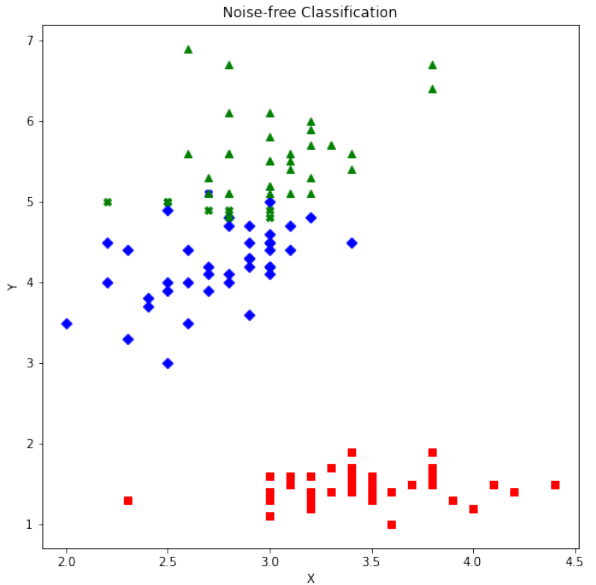


FIG. 7: **Testing the classifier with the ideal simulator.** The overall accuracy is 92.5%. The incorrectly predicted points are marked by \times .

1. Results of noiseless simulations

Figure 5 shows the training curve. As the minimization takes place, the embedded data in \mathcal{H} are expected to form clusters and those from different classes become separated from each other. This is confirmed, as shown in Fig. 6, in the comparison of the overlap of embedded data before and after the training. In particular, the overlaps between the embedded data from different classes become small after the training. This is especially the case for the overlap of class 0 with class 1 and class 2.

After we obtain the optimized circuit parameters, we then use the trained quantum neural network to perform a test on classifying the remaining unused data (i.e. the test data set). Figure 7 shows the classification result on the testing set, still assuming the circuit is noise-free. In the plot, we adopt the convention that the incorrect prediction is marked as ‘ \times ’.

The overall accuracy we obtain is 92.5%. This shows that the classifier can classify unseen data with high accuracy, despite being trained with a relatively small training data set. This, in turn, demonstrates the advantage of this implicit approach, and, hence, the validity of our metric-based framework.

2. Testing results from noisy simulations

In real quantum hardwares, noise and errors are important factors that reduce the accuracy. To examine our method in the presence of noise, we test our classification with noisy models acquired from IBMQ ‘backends’. The

device noise model is generated from their device calibration and takes into account of gate error probability, gate length, T_1 and T_2 relaxation and dephasing times, as well as the readout error probability. For convenience, we show the average gate errors in Table I for the four backends we consider.

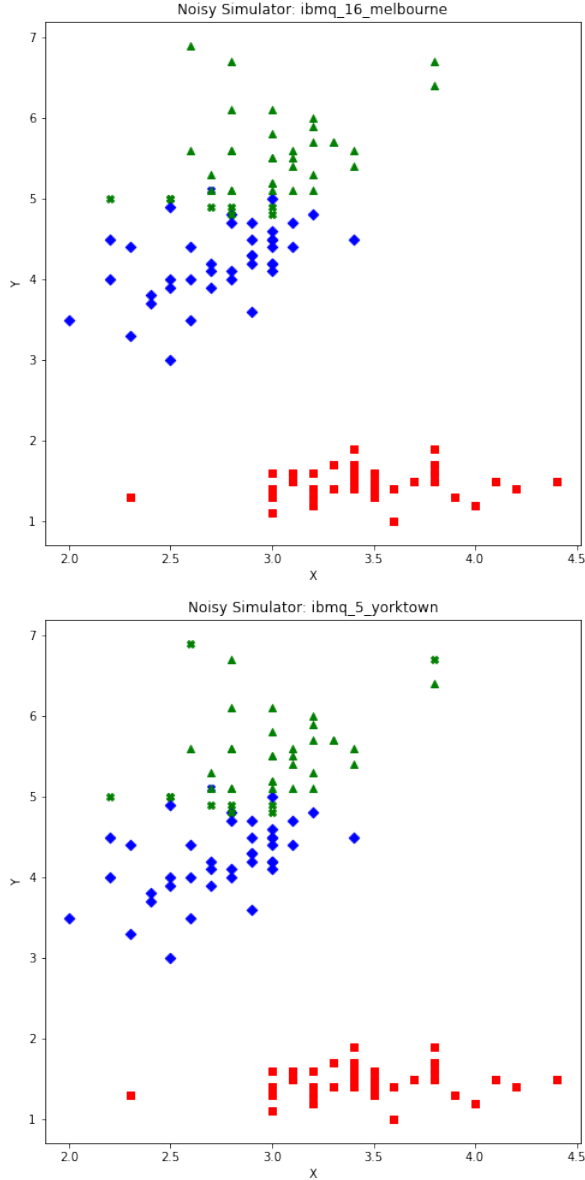


FIG. 8: Testing the classifier with noisy simulators. The noise model is taken from `ibmq_16_melbourne` and `ibmq5_yorktown` devices. The accuracy is 92.5% and 90.83%, respectively.

We test the classification with the SWAP test circuit via the noisy simulations. The results are tabulated in Table I and also presented in Fig. 8 with the noise model from `ibmq_16_melbourne` and `ibmq5_yorktown`, and in Fig. 9 with noise model from `ibmq_rome`. The accuracy seems not affected by the noise and the values from the

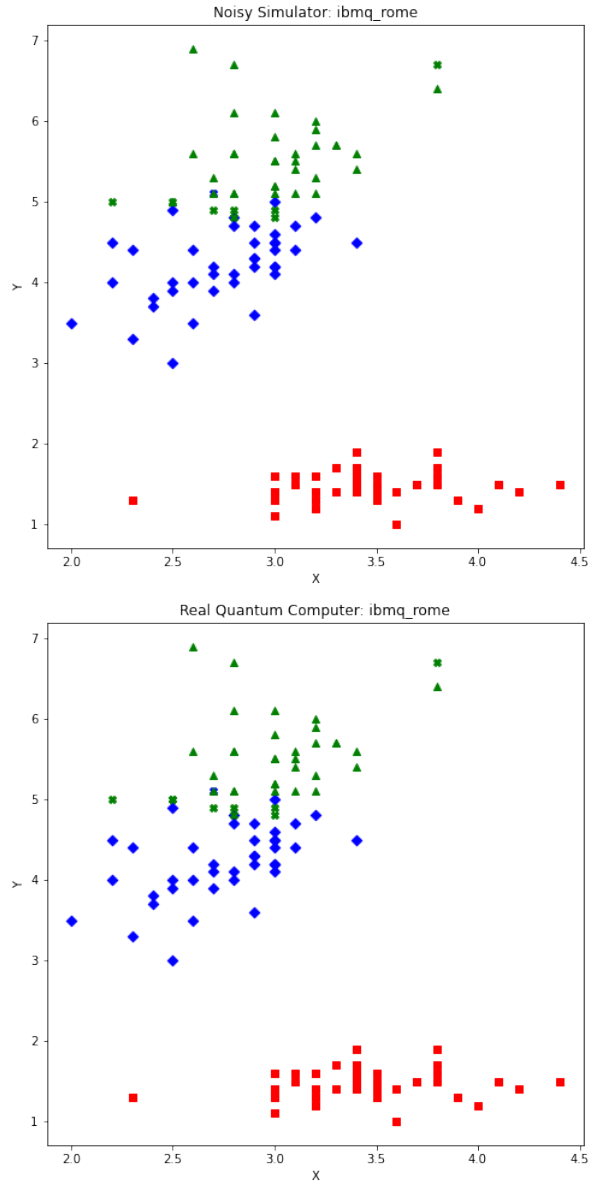


FIG. 9: The top figure shows the result from noisy simulator, with noise modeled from `ibmq_rome`. The bottom figure shows the result from real ‘backends’ `ibmq_rome`. The accuracy is 92.5% and 91.67%, respectively.

two noisy simulations are 90.83%, 92.5% and 92.5%, respectively.

We note that the circuit parameters used are obtained from the noiseless optimization. The reason not to use noisy simulators to obtain the parameters is because we will also perform the same testing on the actual hardware, and it would be impractical and too much time consuming to perform the training directly on the hardware, as the queue of jobs could be long and execution of the training circuits would have to be splitted over many jobs.

	U1 gate error	U2 gate error	U3 gate error	Readout Error	CNOT error	Iris	Circles
<code>ibmq_16_melbourne</code>	0.0	0.00115	0.00229	0.06597	0.03157	92.5%	97%
<code>ibmq5_yorktown</code>	0.0	0.00084	0.00168	0.03494	0.02024	90.83%	93%
<code>ibmq_bogota</code>	0.0	0.00031	0.00062	0.03702	0.01171	92.5%	96%
<code>ibmq_rome</code>	0.0	0.00035	0.00071	0.02397	0.01344	92.5%	95%

TABLE I: **Overall noise properties of 4 machines in our experiment.** For each columns (e.g, ‘U1 gate error’), we average over all the values of each qubit (U1 gate error of all qubits in the machine). For ‘CNOT error rate’, we average over all pairs of qubits. The last two columns show the results of noisy simulations.

3. Some discussions

Correspondence between \mathcal{X} and \mathcal{H} . As described above, the similarity in the input space is expected to be reflected on \mathcal{H} , as the training of quantum circuits would map data classes to well-separated clusters on \mathcal{H} . Our embeddings circuit has 2 qubits, and, hence, the dimension of \mathcal{H} is 4, which cannot be visualized directly. To obtain an illustration of the ‘well-separation’, we adopt the method presented in Ref. [37] and display in Fig. 6 the overlaps between all pairs of training data points, before and after the training process.

Advantage w.r.t measurements: In most of current quantum machine learning models, the outcome of measurement is usually interpreted as the outcome of learning models. In a binary classification problem, one-qubit measurement suffices to classify the data, as there are only two possible outcomes, and one can draw inferences from such measurement. For example, if the probability of obtaining zero $P(\text{outcome} = 0) \geq 0.5$, then we assign the data to class 0. Otherwise we assign it to class 1. For multi-class classification, multi-qubit measurement then needs to be employed. A circuit with k qubits can classify up to 2^k different labels. Our implicit approach surpasses this, as the chosen metric only acts on data points to yield the output metrics vector \vec{f} and one-qubit measurement suffices for the classification. Consider the overlap-metric: for an embedding circuits U with k qubits, it requires $(2k + 1)$ qubits to evaluate the overlaps between two such k -qbit quantum states in the SWAP test subroutine. However, only a single-qubit measurement is needed; see Fig. 4b.

On the other hand, the inversion test requires k qubits and measurement of a simple projector $P_0 = |000..0\rangle\langle 000..0|$; see Fig. 4c. This advantage will be practically useful when the number of qubits is limited (in the near-term era) when the number of labels is large. However, we might not want to ‘pack’ the space with too many labels. The presence of too many classes in the Hilbert space \mathcal{H} might prevent the well-separation of those classes (obtained via training), which in turn decreases the fidelity of the classifier.

C. Run On Quantum Computers

Aside from noisy simulation, we also test our ideally-trained model on real quantum ‘backends’. The result is presented pictorially in Fig. 9 for `ibmq_rome`. Detailed results, including simulations and other devices, are summarized in Table II. For the same classification, we run two different methods to obtain overlaps: (i) the SWAP test, which uses five qubits, and (ii) the inversion test, which uses only two qubits.

The accuracy with ST ranges from 28% to 75% on various backends. However, the accuracy with IT is stably around 90%. They clearly show huge performance difference between the SWAP test and the inversion test. We suspect that the main factor that accounts for such discrepancy is the controlled SWAP gate (c-SWAP in Fig. 4b) in the SWAP test circuit. The number of c-SWAP gates required for two n -qubit states scale as $\mathcal{O}(n)$. Each c-SWAP gate is then decomposed into many CNOT gates (which are noisy), as shown in Fig. 10. Despite the noisy simulations yielding accuracy around 90%, the runs on the actual machines suffer accumulated errors not captured in the noise model and the simulations. Inversion test, on the other hand, does not need the c-SWAP gate, hence, require fewer CNOTs at the cost of doubling the depth of quantum circuit. In our classification model, there is a trade-off between the usage of either the ST or IT. In the NISQ era, as the experiment showed, the inversion test should be used for better classification. However, it requires the ability to invert the embedding circuit and can only evaluate the overlaps between two data points (of pure states). Hence, the process of classifying unseen data (by obtaining metrics vector \vec{f}) must be done in an iterative manner. The SWAP test, on the other hand, can handle mixed states, which can provide speedup with QRAM. We also remark that the performance with SWAP test can be improved further by using methods introduced in [50]. Such approaches rely on classical post-processing to evaluate the state overlaps are hardware-oriented (as the authors examined on IBMQ and Rigetti separately) and requiring fewer CNOT gates.¹

¹ A similar discussion regarding the inversion test and the method in [50] was also presented in [27]. Our experimental work has



FIG. 10: **Decomposition of controlled-SWAP gates into many CNOT and one-qubit gate..** In our work, data is embedded in 2-qubit states. Hence, there are totally 5 qubits in the SWAP test circuit. Note that this picture only shows the decomposition of c-SWAP, not including the data embeddings part. There are 38 CNOT gates used in the decomposition.

IV. EXPLICIT APPROACH

We emphasize that the main idea behind *quantum metric learning* and also our metric-based framework relies on the concept of ‘well-separation’ of data points in \mathcal{H} . A pre-defined metric \mathcal{M} is used to produce such ‘well-separation’ and can be used further to classify unseen data. As mentioned previously, the emphasis of the implicit approach is on the training of the embedding circuit so as to produce separated clusters on \mathcal{H} . However, the ‘centers’ of these clusters are somewhat random. As long as relative distances among these clusters are maximal and those among data points within the same cluster are minimal, the classification still works.

Here we introduce an explicit approach, where the ‘positions’ of clusters are designed to be fixed and separated into orthogonal subspaces. The main intuition is that, with enough qubits, the Hilbert space is a vast complex space that can accommodate many smaller subspaces into which data clusters can reside. These subspaces are well-defined and well-separated. If the data from different classes are ‘approximately’ mapped to their proper subspaces, then they are well-separated by construction. The approximation here means that the embedded data might not lie completely within the desired subspace, but possibly only in its vicinity. (Note that it is impossible for multiple data points to be contained completely in some one-dimensional subspace.) Then, a chosen metric can be employed to measure the distance from a data point on \mathcal{H} to different subspaces, and thus classification of such a data point can be done accordingly.

elaborated this issue further, as we have explicitly examined the performance of SWAP test and inversion test in the presence of noise.

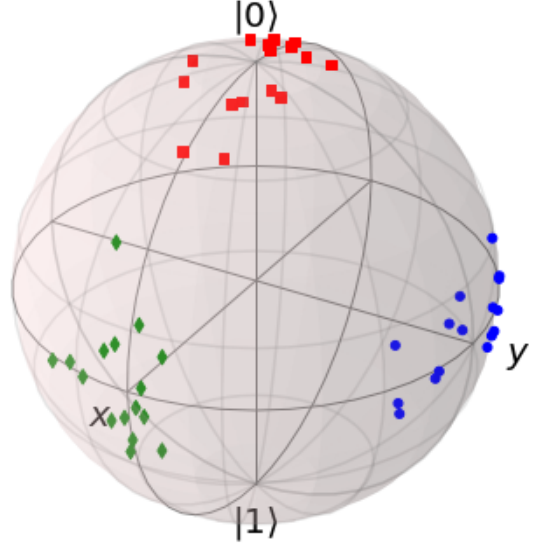


FIG. 11: **Illustration of explicit approach.** The ‘center’ of each clusters are fixed: for class 0 (red points), the position of the center is $v_0 = (0,0,1)$, for class 1 (green points), the position is $v_1 = (1,0,0)$ and for class 2, the position is $v_2 = (0,1,0)$

A. Description

Again, consider the supervised learning problem with M labels, we decompose \mathcal{H} into:

$$\mathcal{H} = H_0 \oplus H_1 \oplus \dots \oplus H_{M-1} \oplus \dots,$$

assuming that $M \leq \dim(\mathcal{H})$. We can always achieve this condition by adding more qubits to the circuits.

Our aim is to approximately map a data point accordingly to its ‘label’ subspace $\{H_i\}$. Without loss of generality, let $\dim(H_i) = k$ and H_i be spanned by $\{|\psi_i^j\rangle\}_{j=1}^k$. Let a set of operators associated to label i , or equiva-

lently, the subspace H_i , be: $\{|\psi_i^j\rangle\langle\psi_i^j|\}_{j=1}^k$. The likelihood of given data $|x\rangle$ having some label i is quantified by the ‘distance’ of $|x\rangle$ to the corresponding ‘label’ subspace. Using overlap-metric, f_i is calculated as:

$$f_i = \sum_{j=1}^k \text{Tr}(|x\rangle\langle x|\psi_i^j\rangle\langle\psi_i^j|) = \text{Tr}(|x\rangle\langle x|\sigma_i) \quad (9)$$

where

$$\sigma_i = \sum_{j=1}^k |\psi_i^j\rangle\langle\psi_i^j|. \quad (10)$$

which could be interpreted as a general operator associated with label i . The metric vector $\vec{f}(x, \theta)$ has the form:

$$\begin{bmatrix} \text{Tr}(|x\rangle\langle x|\sigma_0) \\ \text{Tr}(|x\rangle\langle x|\sigma_1) \\ \vdots \\ \text{Tr}(|x\rangle\langle x|\sigma_{M-1}) \end{bmatrix}. \quad (11)$$

The same strategy is then followed as we minimized the cost in Eq. (1) and assigned some unseen data x according to the value of f_i .

As an example, we consider the binary supervised learning problem with $M = 2$ and 1-dim data set $X = X_A \cup X_B$, where X_A and X_B are the training sets with label 0 and 1, respectively, as depicted in Fig. 12. For simplicity, we use one qubit in the embedding circuit (one can refers to the 1-qubit toy model in [37]). Hence, $\dim \mathcal{H} = 2$. We then make the decomposition:

$$\mathcal{H} = \mathcal{H}_0 \oplus \mathcal{H}_1$$

where \mathcal{H}_0 and \mathcal{H}_1 are spanned by $|0\rangle$ and $|1\rangle$, respectively. The metrics vector \vec{f} has the form:

$$\begin{bmatrix} \text{Tr}(|x\rangle\langle x|\sigma_0) \\ \text{Tr}(|x\rangle\langle x|\sigma_1) \end{bmatrix} = \begin{bmatrix} \text{Tr}(|x\rangle\langle x|\cdot|0\rangle\langle 0|) \\ \text{Tr}(|x\rangle\langle x|\cdot|1\rangle\langle 1|) \end{bmatrix}. \quad (12)$$

Following the same procedure, one obtains the cost value

$$C = 1 - \frac{1}{2} \text{Tr}[\sigma_z(\rho_A - \rho_B)], \quad (13)$$

where ρ_A and ρ_B are state ensembles of the two training sets A and B, respectively, and σ_z is the Pauli-Z matrix. Minimization of this cost C with respect to circuit’s parameters will give us with an embedding $\Phi(x, \theta)$ that maps the data from A to the vicinity of $|0\rangle$ in \mathcal{H} , and the data from B to the vicinity of $|1\rangle$ in \mathcal{H} , as illustrated in Fig. 12.

An alternative picture can be drawn from the above-described 1-dim data set: if we choose label space to be $\{H_0, H_1\}$, then the metrics vector in Eq. 12 can be obtained by simply performing measurement on embedded

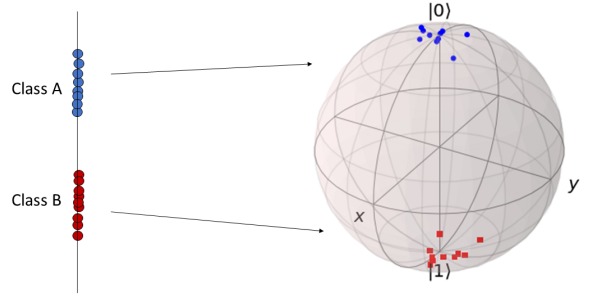


FIG. 12: **Illustration of binary classification.** After training stage, data from A is mapped to blue points, centering around $|0\rangle$. Data from B is mapped to red points, centering around $|1\rangle$. These clusters are well-separated

state $|x\rangle$ in the z basis (i.e., with respect to the observable σ_z of a chosen qubit). If one chose a different label space, for instance, by decomposing $\mathcal{H} = \mathcal{H}_+ \oplus \mathcal{H}_-$, where \mathcal{H}_+ and \mathcal{H}_- are spanned by $(|0\rangle + |1\rangle)/\sqrt{2}$ and $(|0\rangle - |1\rangle)/\sqrt{2}$, respectively, then measurement in the x basis (i.e. the observable σ_x) would need to be used instead. The metrics vector \vec{f} in this latter case is then a direct result from such a σ_x measurement. Instead of the north pole and south pole on the Bloch sphere (see Fig. 12), the training of the quantum circuit would then make data points clustering around “ \hat{x} pole” and “ $-\hat{x}$ pole”, where \hat{x} is the unit vector point along the positive x direction.

Relation to traditional quantum classification model: We give a closer look to metric vector \vec{f} in Eq. (12). The value of $f_0 = \text{Tr}(|x\rangle\langle x|\cdot|0\rangle\langle 0|) = |\langle 0|\cdot|x\rangle|^2$. This turns out to be the probability of obtaining the string 0 when measuring the state $|x\rangle$ in computational basis. Most of current quantum classifiers [26, 27] also rely on such measurement outcomes after applying a general circuit $\Phi(x, \theta) = W(\theta)U(x)$ to some initial state $|00\dots 0\rangle$, for classification. Hence, under the view of embeddings, by choosing appropriate label space (more specifically, standard computational basis state), there is an equivalence between this explicit approach and other traditional models. This fact provides a unified picture of classification on Hilbert space. Such unification is a profound consequence of focusing on representation of embedded data on Hilbert space \mathcal{H} .

The equivalence to traditional models give two-fold advantages: the evaluation of overlaps between the input data $|x\rangle$ and $|\psi_i^j\rangle$ as in Eq. (10) can be done simply by letting x undergo the embedding circuit $\Phi(x, \theta)$ once and perform measurements, instead of invoking the embedding circuit twice (in SWAP test subroutine). Additionally, the evaluation of the cost in Eq. (13) is not necessarily be done in an iterative manner, as in Ref. [45, 51],

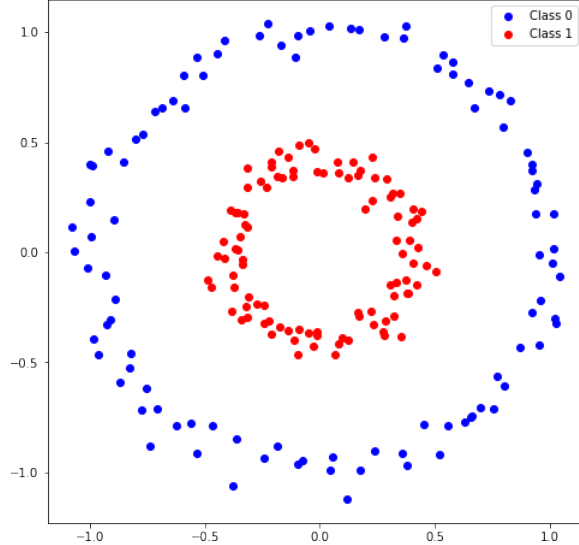


FIG. 13: The Make_circles dataset with $N = 2$ labels. These will be used in our explicit approach for classification.

the authors provided elegant and efficient methods to encoded the cost evaluation directly into quantum circuit. Hence, the training time can be reduced. Of course, we mention that QRAM still can provide speedup in a very similar manner.

B. Numerical Experiments

Datasets: To illustrate this second approach, we target the dataset make_circles with $N = 2$ labels (see Fig. 13). 15 points are taken from each class to serve as training data. For testing, we generate additional 50 points for each class.

Training Stage: We choose two subspaces spanned by $|00\rangle$ and $|11\rangle$ respectively as label spaces, and train the circuit to map data from class 0 (blue points) to H_{00} and map data from class 1 (red points) to H_{11} . Given some input data x , the metrics vector is then:

$$\begin{bmatrix} \text{Tr}(|x\rangle\langle x| \cdot |00\rangle\langle 00|) \\ \text{Tr}(|x\rangle\langle x| \cdot |11\rangle\langle 11|) \end{bmatrix}. \quad (14)$$

The cost function becomes:

$$C = 1 - \frac{1}{2} \left\{ \text{Tr} [\sigma_A (|00\rangle\langle 00| - |11\rangle\langle 11|)] - \text{Tr} [\sigma_B (|00\rangle\langle 00| - |11\rangle\langle 11|)] \right\}, \quad (15)$$

where $\sigma_A = \frac{1}{N_A} \sum_A |x_A\rangle\langle x_A|$, and $\sigma_B = \frac{1}{N_B} \sum_B |x_B\rangle\langle x_B|$. A and B refers to class 0 and 1, respectively.

Results: The training curve in the noiseless simulation is presented in Fig. 14. As in the implicit case, we visual-

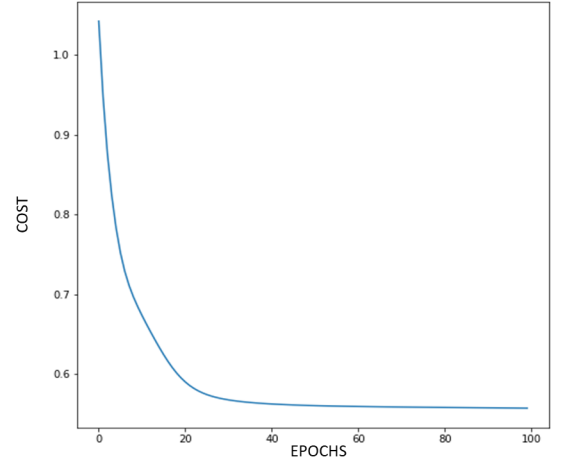


FIG. 14: **Cost as function of epochs.** There are 100 epochs in this training. There are 15 training points for each class and total of 30 training points.

ize the overlaps between training points before and after training with 100 epochs, shown in Fig. 15.

The noiseless testing result is shown in Fig. 16. It is seen that our quantum classifier performs accurately even if it is trained on a relatively small training set.

C. Noisy simulations

As in the previous implicit case, we also use the trained parameters from the noiseless simulation for the quantum embedding, but performs the noisy simulation to classify the testing data set. The noisy classification is presented in Figs. 17, 18, and 19 with noise models from `ibmq_16_melbourne`, `ibmq_5_yorktown` and `ibmq_rome`, respectively. The accuracy of these noisy simulations and another one with the noise model from `ibmq_bogota` is also tabulated in Table II.

D. Run On Quantum Computers

We perform the classification experiments of this explicit approach on real quantum backends `ibmq_16_melbourne`, `ibmq_5_yorktown`, `ibmq_bogota` and `ibmq_rome` and compare their accuracy to the noisy simulation with the noise model from the same backend. The results are summarized in Table II.

The accuracy from the noisy simulators and real machines turns out to agree well with each other, achieving values above 90%. This indicates that this explicit approach is less affected by the noise compared to the implicit approach using the SWAP test. This is reasonable as the explicit approach requires less resource, such as, fewer two-qubit gates than the implicit approach with the SWAP test. We simply let the input data run through the circuit and perform computational-basis measurements,

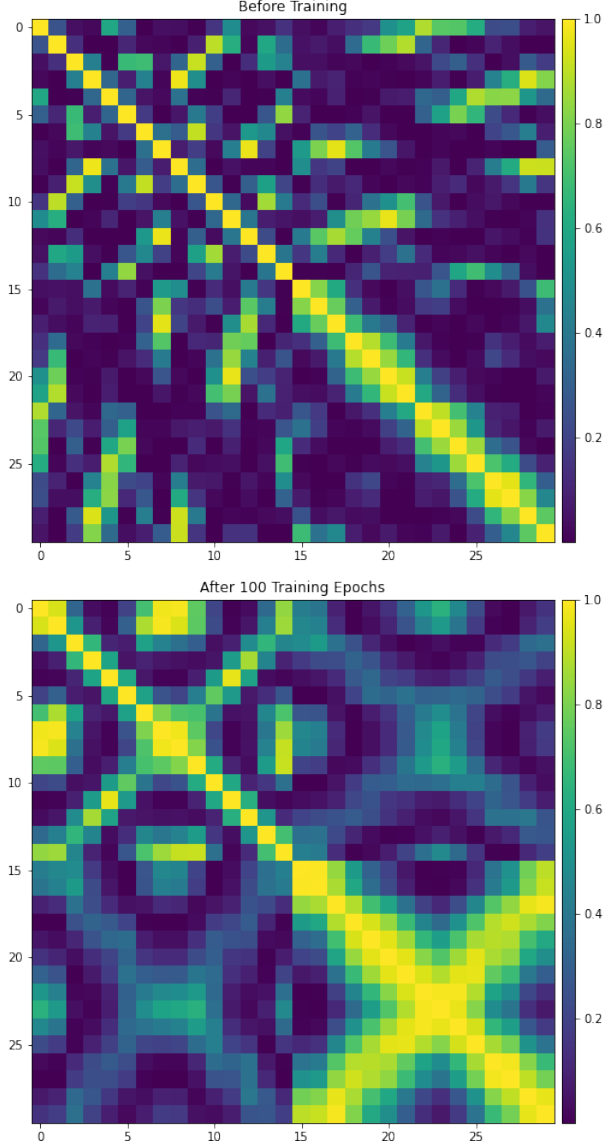


FIG. 15: **Visualization of overlaps between training points (15 training points in each class).**

After training process, data from different classes are getting separated. Compared with implicit approach, the ‘well-separation’ is less apparent, which could be reasonably explained by the way two methods work: in implicit approach, the optimization procedure focuses on *directly* separating data points from different classes, meanwhile in explicit approach, data are getting separated *indirectly*, i.e, through the pre-defined subspaces. Hence, in theory, implicit approach have certain advantage over explicit approach, in terms of attaining complete separation. In practice, both approaches have strong classification ability, as also shown through experiments.

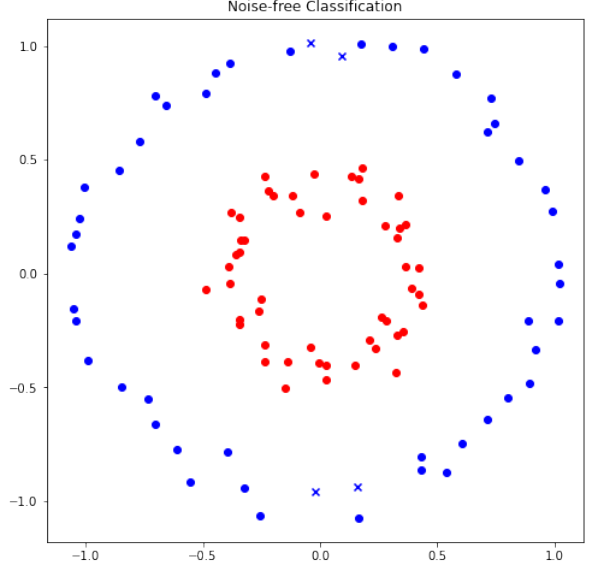


FIG. 16: Testing our explicit quantum classifier with the ideal simulator. The incorrect prediction for class 0 is marked with ‘X’, and for class 1 is ‘+’. The overall accuracy is 96%. Class 1 (red points) were predicted with perfect accuracy. Meanwhile, 4 data from class 0 (blue points) had incorrect prediction.

	Iris	Circles
<i>Ideal simulator</i>	92.5%	96%
<i>ibmq_16_melbourne</i>	92.5% (n.s.) 32.5% (r.d. ST) 88.33% (r.d. IT)	97% (n.s.) 99% (r.d.)
<i>ibmq_5_yorktown</i>	90.83% (n.s.) 50% (r.d. ST) 83.83% (r.d. IT)	93% (n.s.) 91% (r.d.)
<i>ibmq_bogota</i>	92.5% (n.s.) 75% (r.d. ST) 91.67% (r.d. IT)	96% (n.s.) 95% (r.d.)
<i>ibmq_rome</i>	92.5% (n.s.) 28.33% (r.d. ST) 91.67% (r.d. IT)	95% (n.s.) 94% (r.d.)

TABLE II: **Summary of Results:** for simulations and runs on actual backends for both the Iris dataset and the make_circles dataset. The result on the top of each block corresponds to noisy simulation (n.s.), the one on the bottom corresponds to real device (r.d.). ST stands for Swap Test, and IT stands for Inversion Test.

as the classification depends only on the probability of obtaining $|00\rangle$ and $|11\rangle$.

V. PROSPECT IN THE NISQ ERA

Here, we discuss certain perspectives regarding our classification approaches for the NISQ era.

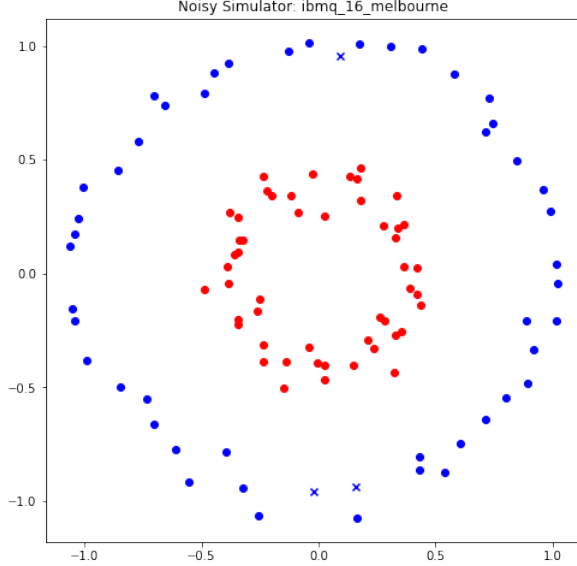


FIG. 17: Testification with noise model taken from `ibmq_16_melbourne` device. The overall accuracy is surprisingly 97%, which is slightly higher than the noise-free case. We attribute this enhancement as an unexpected effect of noise.

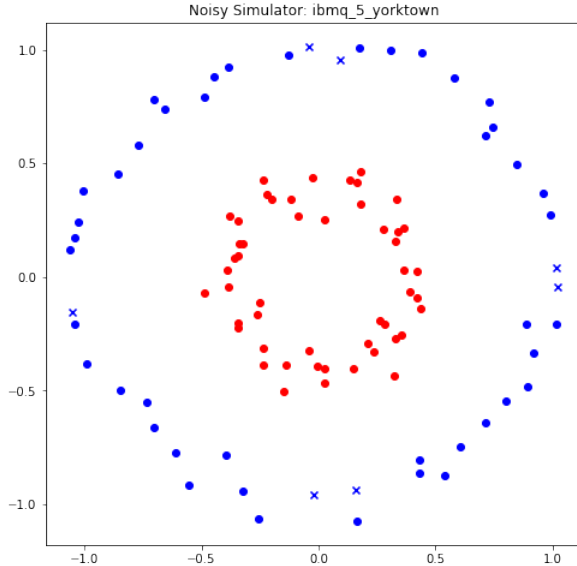


FIG. 18: Noise model taken from `ibmq_5_yorktown` device. The overall accuracy is 93%, which exhibits a slight affect of noise.

A. Classification With Arbitrary Metric

Remind that the classification relies on the metric vector \vec{f} (see Fig. 1), whose components f_i is generally specified by some metric \mathcal{M} . In implicit approach, we base on the overlaps between given data $|x\rangle$ and all points with label i . In explicit approach, we use overlaps between

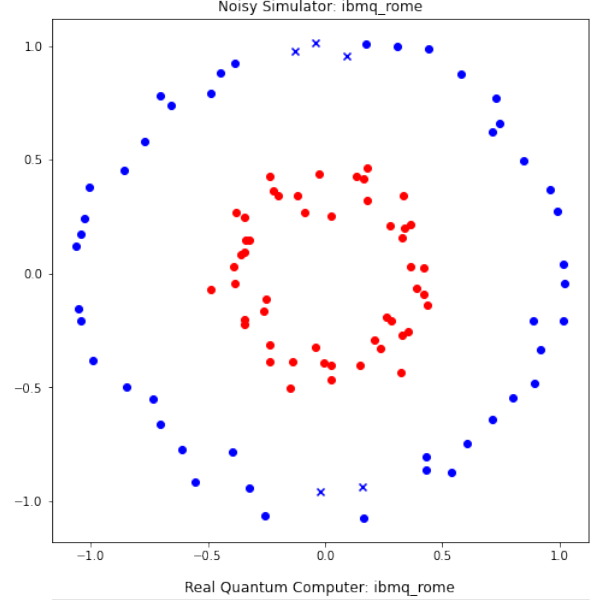


FIG. 19: Top figure: The noise model is taken from `ibmq_rome`. The overall accuracy is 95%, which nearly matches the performance of ideal simulator. Bottom figure: Testing on real ‘backends’ `ibmq_rome`. The overall accuracy is surprisingly 94%, nearly matches the performance of noisy simulator, also ideal simulator.

$|x\rangle$ and the spanning set of chosen ‘label’ subspace. Such overlaps could be extended to arbitrary distance measure, or metric.

A general circuit that computes arbitrary metric would take two quantum states ρ and σ as input, plus possibly some ancilla qubits as well. The fidelity between ρ and σ can then be estimated from the measurement outcome. Throughout this paper, we emphasize the overlap-metric as it requires low-depth circuits, hence being accessible to near-term quantum devices. The overlap-metric also allow us to draw the equivalence between the explicit

approach and other quantum supervised learning model. The value of f_i quantifies the possibility that the given input x belongs to a class $\{i\}$. With overlap-metric, in the implicit approach, the average overlaps can be simplified by taking trace of $|x\rangle\langle x|$, times the ensemble $\{\sigma_i\}$ of quantum states from the corresponding training class. At the moment, such ensembles cannot be directly created in a single circuit and must be obtained by sampling techniques. In Ref. [52], the authors defined the *quantum centroid*, which is a quantum version of centroid vector in classical machine learning. Clearly, such a quantum centroid can be employed in the implicit approach to ‘represent’ the class on the Hilbert space \mathcal{H} . The optimization of the quantum circuit will focus on minimizing the average distance from data points to the corresponding quantum centroid and maximizing the distances between different quantum centroids.

Under different forms of metric, the cost function might be complicated. Moreover, there might not be an efficient way to implement such metric. The overlap-metric, aside from being implementable in the near-term era, also gives rise to a simple cost function as in Eq. (6), for which significant speedup could be gained with the use of a QRAM.

B. Further comments on the prospect

We remark that in order to maximally enhance the performance of any quantum algorithm, or generally a quantum procedure, we also need to take into account of the hardware structure, e.g, the connectivity of qubits in the system and specific qubits chosen. Figure 20 shows the topology of the machine `ibmq_bogota` that we used in our work.

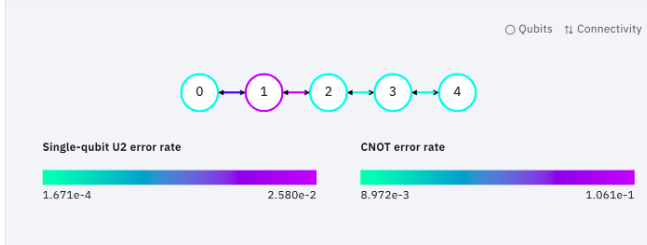


FIG. 20: **Topology of `ibmq_bogota`.** The picture was acquired at the time of our experiment. Topology of other machines that we used in our experiment can be found in Fig. 21.

The result of testing the Iris dataset on `ibmq_bogota` is shown in Table II, with the inversion test done with qubit labeled ‘3’ and ‘4’. We also carried out the same ‘testification’ using qubit ‘1’ and ‘2’. The testification result was only 65.83%, which is dramatically lower than using qubit ‘3’ and ‘4’ (91.67%). Such a deviation can be reasonably argued from the noise rates of the qubit pair involved and of the their CNOT gate. As seen in Fig. 20,

qubits ‘3’ and ‘4’, as well as the connection between them, have much lower error rates, compared to those of qubits ‘1’ and ‘2’. Hence, in practice, any quantum procedure need to be hardware-oriented in order to reach its maximum efficiency. Of course, our experiment requires very few number of qubits and simple gates, so we can simply change or choice of qubits by hand to obtain a better accuracy. More complicated quantum circuits generally require more careful qubit specification. The topology of quantum hardware also varies, e.g, `ibmq_16_melbourne`, `ibmq5_yorktown`, versus `ibmq_bogota`, and such a difference can affect the decomposition of a multi-qubit gate into available one- and in particular two-qubit gates. A hardware-oriented compiler that optimizes the selection is also a necessity for large-scale tasks in the future. We believe that such optimization of hardware-specification is practically important and require further development. Given an arbitrary quantum backend’s topology and description of some quantum procedures, such as circuit’s length, width, number of 1-qubit, 2-qubit gate, one may asks whether or not there exist a systematic procedure that can decide which qubits, and in what orders, should be used, so as to maximize the performance.

VI. CONCLUSION

Highly inspired by the work in [37], our work presents a generic, so-called metric-based framework. The main conceptual tool of our method is the metric-forwarding diagram, where the input data x in ‘forwarded’ to the metric vector \vec{f} and classification can be done accordingly. A hybrid optimization steps is then proceeded to train the circuit. The embedding circuit, after being trained, can map the data from the input space \mathcal{X} to the proper subspaces in \mathcal{H} .

In Ref. [37], the authors put forward an argument that the embedding part of quantum supervised learning model should be trained instead of the measuring part. We explicitly show that training the embedding part is particularly useful, and have many positive consequences. Our framework, in essence, could be regarded as a generalization of the binary classification model presented in Ref. [37] to multi-label case (with implicit approach) and we demonstrate that the model can classify multi-label data. We emphasize that such ability to work directly with multi-class classification could reduce unnecessary training time, which is practically useful in near-term era. We also point out that with implicit approach, the number of separated classes (labels) in supervised learning problem can, ideally, be arbitrary high. We also remark that the ability of our classification model can go beyond classical data classification. Additionally, we show that there is an equivalence between the traditional quantum classification model and our explicit approach. This approach, in the testing stage, does not require access to the training data points in order to reach a decision on classification and hence gives some advantage, in terms

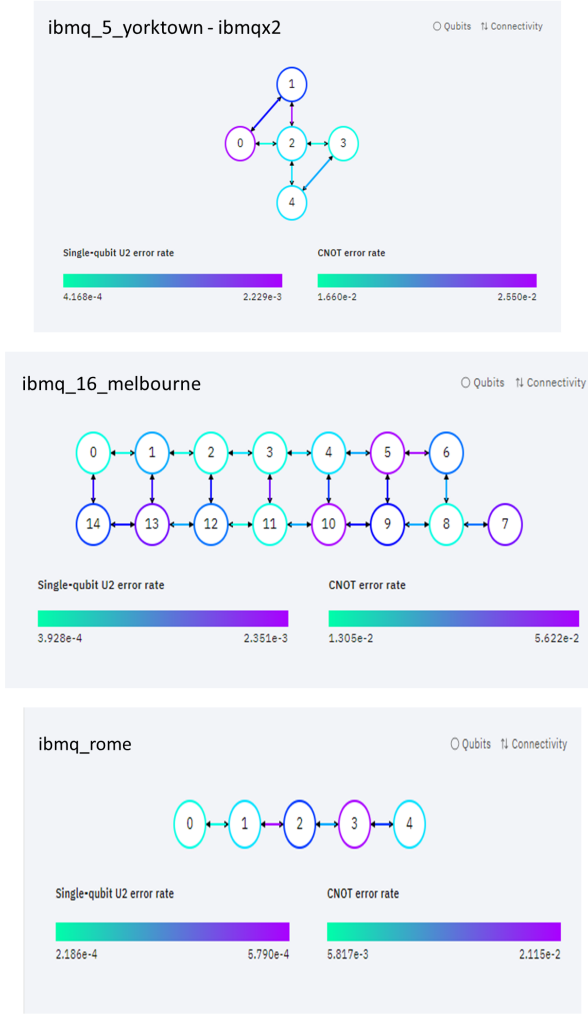


FIG. 21: Topology and the coupling map of `ibmq_5_yorktown`, `ibmq_16_melbourne`, and `ibmq_rome`.

of practical efficiency, over the implicit approach, unless a QRAM exists. The fact that our framework can be divided into explicit and implicit approaches have shown its flexibility, where one can choose in which way data would be embedded and analyzed on the Hilbert space \mathcal{H} . These two approaches constitute to a unified framework for quantum supervised learning.

With overlap-metric, both approaches were shown to be able to classify a sufficiently huge amount of unseen data with high accuracy, even though being trained on a small training set. As we expected, the similarity among same-class data in input space \mathcal{X} is also reflected in Hilbert space \mathcal{H} . Quantum circuit is trained so as to map data from different classes in \mathcal{X} to maximally separated location on \mathcal{H} . Hence, we believe that only a relatively small training points are needed, which has been demonstrated in our experiments. The robustness over small training sizes is more apparent with the implicit approach, since the clusters corresponding to different

classes in \mathcal{H} are *relatively* maximal. We attribute such low-demand on training points as a major advantage of our metric-based framework over other proposed quantum classification models. The fact that our classification model performs well with a small training pool can give rise to further advantages; for example, the training times (or equivalently the number of epochs) can be reduced and this, in turn, can avoid possible overfitting. Aside from being used for classification, we finally note that the trained quantum circuit can probably be used as subroutines of other quantum machine learning algorithms, as we know with high confidence that the embedded data from different classes are well-separated from each other (trained with the implicit approach) or approximately well-contained in some subspaces in \mathcal{H} (trained with the explicit approach).

A few other works have been demonstrating the ability and feasibility of using actual quantum computer to classify real-world data [27, 53]. Aside from providing a unified framework for quantum supervised learning, we have performed simulations and cloud-based real-device experiments. These experiments on real quantum ‘backends’ have also pushed the prospect of applying quantum computers for machine learning one step further, as we have demonstrated explicitly that current noisy quantum computers can still achieve high accuracy on classifying data. The low-accuracy results obtained via the SWAP test routine could be improved by using the inversion test routine, and we have emphasized that the IT is more appropriate in the NISQ era. Real quantum systems are undoubtedly more complicated and their noise on long circuits (especially those with many CNOTs) could result in worse accuracy than noisy simulations. The error rate of 1-qubit gates is $\sim 10^{-3}$ or smaller, and that of the 2-qubit CNOT is $\sim 10^{-3}$ for current hardwares [54]. Full implementation of quantum error correction is still currently not available. Alongside the development of precise, high fidelity gates, efforts have been made towards error mitigation methods [55–58] in order to obtain useful outcomes. Some of these mitigation methods require repetition of the same circuit but with different overall error rates by possibly stretching the gate pulses. This allows observables to be extrapolated to the gate noiseless limit [55, 56]. Measurement error mitigation is also necessary to infer correct readout outcomes [57, 58]. The experiments done in our work do not employ any mitigation technique. We believe that our results can be further improved further with mitigation, especially the results from the SWAP test by using gate mitigation. Additionally, as mentioned previously, our classification model can work well with a small training pool, achieving very high accuracy in testing unseen data. The experiments (numerical or real-device) have shown this advantage. Hence, one can reasonably suspect that the model can be trained on real machines and obtain a comparable performance.

Acknowledgements

We acknowledge use of the IBM Q for this work. The views expressed are those of the authors and do not reflect the official policy or position of IBM or the IBM Q team. This research used resources of the Oak Ridge Leadership Computing Facility, which is a DOE Office of Science User Facility supported under Contract DE-AC05-00OR22725. This work was partially supported by the U.S. Department of Energy, Office of Science, Office of High Energy Physics program under Award Number DE-SC-0012704 (S.Y.-C.C.), the Brookhaven National Laboratory LDRD #20-024 (S.Y.-C.C.), and a subcontract No. 384153 from Brookhaven Science Associates LLC (T.-C.W.).

Appendix A: Implicit Approach and Hilbert-Schmidt Distance

Consider the binary supervised learning problem ($N=2$) under implicit approach. Denote two classes as A and B. The metric vector \vec{f} now have the form

$$\begin{bmatrix} \text{Tr}(|x\rangle\langle x|\sigma_A) \\ \text{Tr}(|x\rangle\langle x|\sigma_B) \end{bmatrix}$$

Using Eq. (1), the cost function becomes

$$C = 1 - \frac{1}{2} \sum_A^B \text{Tr}(\sigma_i^2) + \text{Tr}(\sigma_A \sigma_B) = 1 - \frac{1}{2} \text{Tr}((\sigma_A - \sigma_B)^2) \quad (\text{A1})$$

Hence, maximizing the Hilbert-Schmidt distance $D = \text{Tr}((\sigma_A - \sigma_B)^2)$ between two data classes minimizes the cost, as highlighted in [37].

We assign x to class A if $f_A > f_B$, or equivalently, $f_A - f_B > 0$. We also have: $f_A = \text{Tr}(|x\rangle\langle x|\sigma_A) = \langle x|\sigma_A|x\rangle$ and $f_B = \text{Tr}(|x\rangle\langle x|\sigma_B) = \langle x|\sigma_B|x\rangle$. The criteria $f_A - f_B > 0$ is then can be written as

$$\langle x|(\sigma_A - \sigma_B)|x\rangle > 0.$$

The quantity $\langle x|(\sigma_A - \sigma_B)|x\rangle$ is mentioned in [37] as fidelity measurement.

Appendix B: Comments on Trace Distance

In Ref. [37], the authors also defined another type of measurement called Helstrom measurement. Two state ensembles corresponding to two classes A and B are:

$$\sigma_+ = \sum_+ |x_+\rangle\langle x_+|,$$

$$\sigma_- = \sum_- |x_-\rangle\langle x_-|,$$

where $+/ -$ refers to the *positive* and *negative* subspaces of $\sigma_A - \sigma_B$, respectively. Following the same procedure (as in the Hilbert-Schmidt distance case), the cost function is then

$$C = 1 - \frac{1}{2} \text{Tr}[\sigma_A - \sigma_B].$$

Hence, the training of quantum circuit would focus on maximizing the trace distance between two data classes. We remark this method only work in binary classification case ($N=2$) due to the special properties of arbitrary density state ρ : ρ is a Hermitian matrix (can be diagonalized, eigenvalues are real and positive, eigenstates are orthogonal) and has trace 1 (hence, the values of eigenvalue $\{\lambda_i\}$ are bounded between 0 and 1). An extension of this method to multi-class turns out not to be straightforward, and possibly impossible.

Appendix C: One-versus-all Strategy

One-versus-all strategy (Fig. 22) has been used a lot in practice to transform a binary classifier to multi-class classifier, especially for those model that, in essence, can only deal with binary classification. The systematic issue with this strategy has been presented many times in classical machine learning context. Here we review this issue and point out an advantage of focusing on training of embeddings part in quantum supervised learning.

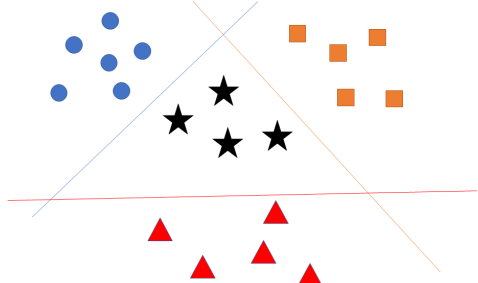


FIG. 22: **One-versus-all Strategy.** There are three classes (blue, orange, and red colors) and the corresponding decision boundary (blue, orange, and red lines). All classes are linearly separable, for simplicity

The caveat of one-versus-all strategy is clear from Fig. 22: the black stars (unseen data) are struggling to find its class (label). A very similar issue would appear in quantum supervised learning, where the data are embedded by a fixed circuit in Hilbert space \mathcal{H} , then the variational circuit is trained to draw the decision boundary. We remark that the training of embeddings part can surpass this issue naturally, as the representation of data in \mathcal{H} is learnt. Then a metric is employed to compare data, a method which is essentially similar to distance-based

approach in classical machine learning context. Hence, a

label for unseen data is always guaranteed.

[1] Michael A Nielsen and Isaac Chuang. Quantum computation and quantum information, 2002.

[2] Aram W Harrow and Ashley Montanaro. Quantum computational supremacy. *Nature*, 549(7671):203–209, 2017.

[3] Hans J Briegel, David E Browne, Wolfgang Dür, Robert Raussendorf, and Maarten Van den Nest. Measurement-based quantum computation. *Nature Physics*, 5(1):19–26, 2009.

[4] Robert Raussendorf and Tzu-Chieh Wei. Quantum computation by local measurement. *Annu. Rev. Condens. Matter Phys.*, 3(1):239–261, 2012.

[5] Peter W Shor. Polynomial-time algorithms for prime factorization and discrete logarithms on a quantum computer. *SIAM review*, 41(2):303–332, 1999.

[6] Lov K Grover. A fast quantum mechanical algorithm for database search. In *Proceedings of the twenty-eighth annual ACM symposium on Theory of computing*, pages 212–219, 1996.

[7] Karen Simonyan and Andrew Zisserman. Very deep convolutional networks for large-scale image recognition. In *International Conference on Learning Representations*, 2015.

[8] Christian Szegedy, Wei Liu, Yangqing Jia, Pierre Sermanet, Scott Reed, Dragomir Anguelov, Dumitru Erhan, Vincent Vanhoucke, and Andrew Rabinovich. Going deeper with convolutions. In *Proceedings of the IEEE conference on computer vision and pattern recognition*, pages 1–9, 2015.

[9] Athanasios Voulodimos, Nikolaos Doulamis, Anastasios Doulamis, and Eftychios Protopapadakis. Deep Learning for Computer Vision: A Brief Review. *Computational Intelligence and Neuroscience*, 2018:1–13, 2018.

[10] Ilya Sutskever, Oriol Vinyals, and Quoc V Le. Sequence to sequence learning with neural networks. In *Advances in neural information processing systems*, pages 3104–3112, 2014.

[11] Jessica Vamathevan, Dominic Clark, Paul Czodrowski, Ian Dunham, Edgardo Ferran, George Lee, Bin Li, Anant Madabhushi, Parantu Shah, Michaela Spitzer, et al. Applications of machine learning in drug discovery and development. *Nature Reviews Drug Discovery*, 18(6):463–477, 2019.

[12] David Silver, Aja Huang, Chris J. Maddison, Arthur Guez, Laurent Sifre, George van den Driessche, Julian Schrittwieser, Ioannis Antonoglou, Veda Panneershelvam, Marc Lanctot, Sander Dieleman, Dominik Grewe, John Nham, Nal Kalchbrenner, Ilya Sutskever, Timothy Lillicrap, Madeleine Leach, Koray Kavukcuoglu, Thore Graepel, and Demis Hassabis. Mastering the game of Go with deep neural networks and tree search. *Nature*, 529(7587):484–489, 1 2016.

[13] Jacob Biamonte, Peter Wittek, Nicola Pancotti, Patrick Rebentrost, Nathan Wiebe, and Seth Lloyd. Quantum machine learning. *Nature*, 549(7671):195–202, 2017.

[14] Peter Wittek. *Quantum machine learning: what quantum computing means to data mining*. Academic Press, 2014.

[15] Maria Schuld. Machine learning in quantum spaces, 2019.

[16] Vedran Dunjko and Hans J Briegel. Machine learning & artificial intelligence in the quantum domain: a review of recent progress. *Reports on Progress in Physics*, 81(7):074001, 2018.

[17] Esma Aïmeur, Gilles Brassard, and Sébastien Gambs. Quantum speed-up for unsupervised learning. *Machine Learning*, 90(2):261–287, 2013.

[18] JS Otterbach, R Manenti, N Alidoust, A Bestwick, M Block, B Bloom, S Caldwell, N Didier, E Schuyler Fried, S Hong, et al. Unsupervised machine learning on a hybrid quantum computer. *arXiv preprint arXiv:1712.05771*, 2017.

[19] Nathan Wiebe, Ashish Kapoor, and Krysta Svore. Quantum algorithms for nearest-neighbor methods for supervised and unsupervised learning. *arXiv preprint arXiv:1401.2142*, 2014.

[20] Seth Lloyd, Masoud Mohseni, and Patrick Rebentrost. Quantum algorithms for supervised and unsupervised machine learning. *arXiv preprint arXiv:1307.0411*, 2013.

[21] Iordanis Kerenidis, Jonas Landman, Alessandro Luongo, and Anupam Prakash. q-means: A quantum algorithm for unsupervised machine learning. In *Advances in Neural Information Processing Systems*, pages 4134–4144, 2019.

[22] Maria Schuld and Francesco Petruccione. *Supervised learning with quantum computers*, volume 17. Springer, 2018.

[23] Marcello Benedetti, Erika Lloyd, Stefan Sack, and Mattia Fiorentini. Parameterized quantum circuits as machine learning models. *Quantum Science and Technology*, 4(4):043001, 2019.

[24] Patrick Rebentrost, Masoud Mohseni, and Seth Lloyd. Quantum support vector machine for big data classification. *Physical review letters*, 113(13):130503, 2014.

[25] Edward Farhi and Hartmut Neven. Classification with quantum neural networks on near term processors. *arXiv preprint arXiv:1802.06002*, 2018.

[26] Maria Schuld, Alex Bocharov, Krysta M Svore, and Nathan Wiebe. Circuit-centric quantum classifiers. *Physical Review A*, 101(3):032308, 2020.

[27] Vojtěch Havlíček, Antonio D Córcoles, Kristan Temme, Aram W Harrow, Abhinav Kandala, Jerry M Chow, and Jay M Gambetta. Supervised learning with quantum-enhanced feature spaces. *Nature*, 567(7747):209–212, 2019.

[28] Kosuke Mitarai, Makoto Negoro, Masahiro Kitagawa, and Keisuke Fujii. Quantum circuit learning. *Physical Review A*, 98(3):032309, 2018.

[29] Yann LeCun, Yoshua Bengio, and Geoffrey Hinton. Deep learning. *nature*, 521(7553):436–444, 2015.

[30] Alex Krizhevsky, Ilya Sutskever, and Geoffrey E Hinton. Imagenet classification with deep convolutional neural networks. In *Advances in neural information processing systems*, pages 1097–1105, 2012.

[31] Edward Grant, Marcello Benedetti, Shuxiang Cao, Andrew Hallam, Joshua Lockhart, Vid Stojovic, Andrew G Green, and Simone Severini. Hierarchical quantum classifiers. *npj Quantum Information*, 4(1):1–8, 2018.

[32] Yuxuan Du, Min-Hsiu Hsieh, Tongliang Liu, Shan You, and Dacheng Tao. On the learnability of quantum neural

networks. *arXiv preprint arXiv:2007.12369*, 2020.

[33] Maria Schuld and Nathan Killoran. Quantum machine learning in feature hilbert spaces. *Physical review letters*, 122(4):040504, 2019.

[34] Maria Schuld, Ryan Sweke, and Johannes Jakob Meyer. The effect of data encoding on the expressive power of variational quantum machine learning models. *arXiv preprint arXiv:2008.08605*, 2020.

[35] Samuel Yen-Chi Chen, Chao-Han Huck Yang, Jun Qi, Pin-Yu Chen, Xiaoli Ma, and Hsi-Sheng Goan. Variational quantum circuits for deep reinforcement learning. *IEEE Access*, 8:141007–141024, 2020.

[36] Samuel Yen-Chi Chen, Shinjae Yoo, and Yao-Lung L Fang. Quantum long short-term memory. *arXiv preprint arXiv:2009.01783*, 2020.

[37] Seth Lloyd, Maria Schuld, Aroosa Ijaz, Josh Izaac, and Nathan Killoran. Quantum embeddings for machine learning. *arXiv preprint arXiv:2001.03622*, 2020.

[38] Sumit Chopra, Raia Hadsell, and Yann LeCun. Learning a similarity metric discriminatively, with application to face verification. In *2005 IEEE Computer Society Conference on Computer Vision and Pattern Recognition (CVPR'05)*, volume 1, pages 539–546. IEEE, 2005.

[39] Maria Schuld, Ilya Sinayskiy, and Francesco Petruccione. The quest for a quantum neural network. *Quantum Information Processing*, 13(11):2567–2586, 2014.

[40] Patrick Rebentrost, Thomas R Bromley, Christian Weedbrook, and Seth Lloyd. Quantum hopfield neural network. *Physical Review A*, 98(4):042308, 2018.

[41] Iris Cong, Soonwon Choi, and Mikhail D Lukin. Quantum convolutional neural networks. *Nature Physics*, 15(12):1273–1278, 2019.

[42] Kerstin Beer, Dmytro Bondarenko, Terry Farrelly, Tobias J Osborne, Robert Salzmann, Daniel Scheiermann, and Ramona Wolf. Training deep quantum neural networks. *Nature communications*, 11(1):1–6, 2020.

[43] Adrián Pérez-Salinas, Alba Cervera-Lierta, Elies Gil-Fuster, and José I Latorre. Data re-uploading for a universal quantum classifier. *Quantum*, 4:226, 2020.

[44] Vittorio Giovannetti, Seth Lloyd, and Lorenzo Maccone. Quantum random access memory. *Physical review letters*, 100(16):160501, 2008.

[45] Shuxiang Cao, Leonard Wossnig, Brian Vlastakis, Peter Leek, and Edward Grant. Cost-function embedding and dataset encoding for machine learning with parametrized quantum circuits. *Physical Review A*, 101(5):052309, 2020.

[46] Ronald A Fisher. The use of multiple measurements in taxonomic problems. *Annals of eugenics*, 7(2):179–188, 1936.

[47] Edgar Anderson. The species problem in iris. *Annals of the Missouri Botanical Garden*, 23(3):457–509, 1936.

[48] Ville Bergholm, Josh Izaac, Maria Schuld, Christian Gogolin, Carsten Blank, Keri McKiernan, and Nathan Killoran. PennyLane: Automatic differentiation of hybrid quantum-classical computations. *arXiv preprint arXiv:1811.04968*, 2018.

[49] T. Tieleman and G. Hinton. Lecture 6.5—RmsProp: Divide the gradient by a running average of its recent magnitude. COURSERA: Neural Networks for Machine Learning, 2012.

[50] Lukasz Cincio, Yiğit Subaşı, Andrew T Sornborger, and Patrick J Coles. Learning the quantum algorithm for state overlap. *New Journal of Physics*, 20(11):113022, 2018.

[51] Soumik Adhikary. An entanglement enhanced training algorithm for supervised quantum classifiers. *arXiv preprint arXiv:2006.13302*, 2020.

[52] Nana Liu and Patrick Rebentrost. Quantum machine learning for quantum anomaly detection. *Physical Review A*, 97(4):042315, 2018.

[53] Carsten Blank, Daniel K Park, June-Koo Kevin Rhee, and Francesco Petruccione. Quantum classifier with tailored quantum kernel. *npj Quantum Information*, 6(1):1–7, 2020.

[54] John Preskill. Quantum computing in the nisq era and beyond. *Quantum*, 2:79, 2018.

[55] Kristan Temme, Sergey Bravyi, and Jay M Gambetta. Error mitigation for short-depth quantum circuits. *Physical review letters*, 119(18):180509, 2017.

[56] Suguru Endo, Simon C Benjamin, and Ying Li. Practical quantum error mitigation for near-future applications. *Physical Review X*, 8(3):031027, 2018.

[57] Yanzhu Chen, Maziar Farahzad, Shinjae Yoo, and Tzu-Chieh Wei. Detector tomography on ibm 5-qubit quantum computers and mitigation of imperfect measurement. *arXiv: Quantum Physics*, 2019.

[58] Sergey Bravyi, Sarah Sheldon, Abhinav Kandala, David C Mckay, and Jay M Gambetta. Mitigating measurement errors in multi-qubit experiments. *arXiv preprint arXiv:2006.14044*, 2020.